

Space-Time-Frequency Code Implementation in MB-OFDM UWB Communications: Design Criteria and Performance

Le Chung Tran and Alfred Mertins

Abstract— This paper proposes a general framework of Space-Time-Frequency Codes (STFCs) for Multi-Band Orthogonal Frequency Division Multiplexing (MB-OFDM) Ultra-Wide Band (UWB) communications systems. A great similarity between the STFC MB-OFDM UWB systems and conventional wireless Complex Orthogonal Space-Time Block Code (CO STBC) Multiple-Input Multiple-Output (MIMO) systems is discovered. This allows us to quantify the pairwise error probability (PEP) of the proposed system and derive the general decoding method for the implemented STFCs. Based on the theoretical analysis results of PEP, we can further quantify the diversity order and coding gain of MB-OFDM UWB systems, and derive the design criteria for STFCs, namely diversity gain criterion and coding gain criterion. The maximum achievable diversity order is found to be the product of the number of transmit antennas, the number of receive antennas, and the FFT size. We also show that all STFCs constructed based on the conventional CO STBCs can satisfy the diversity gain criterion. Various baseband simulation results are shown for the Alamouti code and a code of order 8. Simulation results indicate the significant improvement achieved in the proposed STFC MB-OFDM UWB systems, compared to the conventional MB-OFDM UWB ones.

Index Terms— UWB, MB-OFDM, STFC, MIMO, STC, CO STBC, design criteria, diversity order, coding gain.

I. INTRODUCTION

Recently, Ultra-Wide Band (UWB) communications attracts intensive attention from both industries and researchers, because it is a potential candidate for short-range communications (up to 10 meters) with very high data rate, very low power consumption and emission. UWB can be a baseband system using carrier-free communications, which is referred to as *impulse* UWB, or a carrier-based system. The latter possesses a number of advantages, compared to the former, in terms of low complexity of receivers to capture sufficient multipath energy, and in easier radio frequency (RF) design. One of the main candidates for carrier-based UWB communications is Multi-Band Orthogonal Frequency Division Multiplexing (MB-OFDM), supported by the WiMedia Alliance [1]. MB-OFDM UWB is designed for very high bit rate up to 480 Mbps with low cost and low power consumption.

On the other hand, one of the emerging techniques to resolve the bottleneck of traffic capacity in wireless networks is the use of Multiple-Input Multiple-Output (MIMO) systems. Communication theory [2], [3], [4] shows that MIMO systems can provide potentially a very high capacity that, in

many cases, grows approximately linearly with the number of antennas, without paying any additional power. The main feature of MIMO systems is space-time processing. Space-Time Codes (STCs) are the codes designed for the use in MIMO systems. In STCs, signals are coded in both temporal and spatial domains. Among a variety of STCs, of particular interest are Complex Orthogonal Space-Time Block Codes (CO STBCs), which possess a simpler decoding method than other STCs, such as Space-Time Trellis Codes (STTCs) [5].

Intuitively, the combination of the emerging technologies MB-OFDM UWB, MIMO, and STCs will provide a significant improvement in the maximum achievable communications range, bit error performance, system capacity, and data rate. While the combination of OFDM, MIMO and STCs in the form of Space-Time-Frequency Codes (STFCs) in MIMO-OFDM systems (usually referred to as STFC-MIMO-OFDM systems) has been well examined in the literature, such as [6], [7], [8], [9], [10], the combination of MB-OFDM UWB, MIMO, and STCs has been almost unexplored with few papers examining this issue [11], [12], [13], [14]. There are two main differences between channels' characteristics in conventional OFDM systems and in MB-OFDM UWB ones. First, channels in the conventional OFDM system are less dispersive than those in the MB-OFDM UWB system, due to the fact that the latter has much larger bandwidth. Second, channel coefficients in the conventional OFDM system are usually considered to be Rayleigh distributed, while those in the MB-OFDM UWB system are log-normally distributed [15]. Therefore, the systems incorporating MB-OFDM UWB, MIMO, and STCs must be more specifically analyzed, though there exist some similarities between them and the conventional STFC-MIMO-OFDM systems.

The combination of MB-OFDM UWB systems with STBCs has been somewhat mentioned in [11] for only two transmit (Tx) antennas, i.e. the Alamouti code [16]. In [12], the authors proposed a general framework to analyze the performance of MB-OFDM MIMO UWB systems regardless of specific coding schemes. They quantify the performance of the MB-OFDM MIMO UWB systems in case of Nakagami frequency-selective fading channels. The authors also showed that the maximum achievable diversity of a MB-OFDM MIMO UWB system is the product of the number of Tx and receive (Rx) antennas, the number of multipath components, and the number of jointly encoded OFDM symbols.

However, the multipath channel amplitudes in MB-OFDM UWB systems are independent log-normally distributed ran-

This work has been done under the postdoctoral research fellowship from the Alexander von Humboldt (AvH) Foundation, Germany.

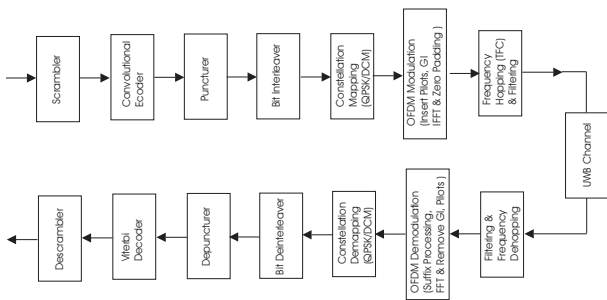


Fig. 1. MB-OFDM UWB system according to WiMedia's specification.

dom variables, rather than Nakagami-distributed [15]. While [12] is a very interesting paper and has significant contribution, it still has some drawbacks, including: a) not quantifying the Pairwise Error Probability (PEP) in the case of log-normal distribution, b) assuming that the time delay and average power are the same for all transmit-receive links in order to calculate the matrix of channel frequency responses, which is not usually true in MB-OFDM systems where the time delay and average power of transmit-receive links might be very different, and c) misjudging that the product between the channel's multipath length and the number of Tx antennas is usually smaller than the FFT size, resulting in an erroneous conclusion that the maximum achievable diversity of MB-OFDM UWB systems is the product of the number of Tx and Rx antennas, the number of multipath components, and the number of jointly encoded OFDM symbols. In fact, the product between the channel's multipath length and the number of Tx antennas is usually much greater than the FFT size, due to the fact that UWB channels are very richly dispersive.

In this paper, we expand the discussion in [11] to propose the STFC MB-OFDM UWB system for any number of Tx/Rx antennas. We follow an approach, independently of the existing works, to examine the performance of STFC MB-OFDM UWB systems. In particular, we modify the Tarokh's proof, which was mentioned in [5] for the conventional wireless STC MIMO communications, to find the diversity and coding gains of the proposed STFC MB-OFDM UWB system in the log-normal distribution case [17], without any restriction or additional assumption on the time delay and average power of transmit-receive links. Our analysis is based closely on WiMedia's MB-OFDM UWB PHY specifications and the IEEE 802.15.3a UWB channel model. We discover that the maximum achievable diversity gain of the proposed STFC MB-OFDM UWB system is the product of the numbers of Tx and Rx antennas and the FFT size. The paper also derives the decoding algorithm for general STFCs, and then considers the Alamouti code and our order-8 code proposed in [18] for illustration. Several simulation results for the Alamouti code and the order-8 code with QPSK and Dual Carrier Modulation (DCM) schemes are shown in order to verify the performance improvement of the proposed STFC MB-OFDM UWB systems, compared to the conventional MB-OFDM ones.

The paper is organized as follows. In Section II, we review WiMedia's MB-OFDM UWB PHY specifications and the

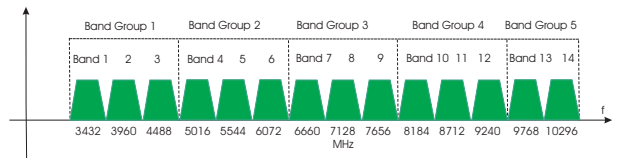


Fig. 2. MB-OFDM UWB band groups.

IEEE 802.15.3a UWB channel model. In Section III, we propose the STFC MB-OFDM UWB system for any number of Tx/Rx antennas as well as the mathematical model for the proposed system. Section IV analyzes the diversity gain and coding gain of the proposed STFC MB-OFDM system under the WiMedia's UWB MB-OFDM PHY specifications and the IEEE 802.15.3a UWB channel model. Section V provides two main criteria to design STFCs in MB-OFDM UWB systems, namely diversity gain criterion and coding gain criterion. In Section VI, we derive the general Maximum Likelihood (ML) decoding expression for STFCs and the detailed decoding metrics for the Alamouti code and our order-8 code. Simulation results are mentioned in Section VII and conclusions are drawn in Section VIII.

Notations: The following notations will be used throughout the paper. The superscripts $(\cdot)^*$, $(\cdot)^T$ and $(\cdot)^H$ denote the complex conjugation, transposition operation, and Hermitian transpose operation, respectively. We denote $\bar{\mathbf{a}} \otimes \bar{\mathbf{b}}$, $\bar{\mathbf{a}} * \bar{\mathbf{b}}$, and $\bar{\mathbf{a}} \bullet \bar{\mathbf{b}}$ to be the *linear convolution*, the *cyclic (or circular) convolution*, and the element-wise (or Hadamard) product of the two vectors $\bar{\mathbf{a}}$ and $\bar{\mathbf{b}}$, respectively. Further, $\bar{\mathbf{a}}.^2$ denotes the element-wise power-2 operation of $\bar{\mathbf{a}}$. We define the multiplication operation $\mathbf{C} \circ \mathbf{D}$ between the two matrices $\mathbf{C} = \{\bar{\mathbf{c}}_{t,m}\}_{T \times M}$ and $\mathbf{D} = \{\bar{\mathbf{d}}_{m,n}\}_{M \times N}$, whose elements $\bar{\mathbf{c}}_{t,m}$ and $\bar{\mathbf{d}}_{m,n}$ are N_{fft} -length column vectors, such that the (t,n) -th element of the resulting matrix is a N_{fft} -length column vector $\sum_{m=1}^M \bar{\mathbf{c}}_{t,m} \bullet \bar{\mathbf{d}}_{m,n}$. The complex space \mathcal{C} of a symbol s denotes all potential possibilities that the symbol s can take, while the N_D -dimensional complex space \mathcal{C}^{N_D} of a N_D -length vector $\bar{\mathbf{s}}$ denotes all potential possibilities that the vector $\bar{\mathbf{s}}$ can take. We define $\bar{\mathbf{1}}$ as a column vector of length N_D , whose elements are all 1. Finally, $\|\cdot\|_F$ denotes the Frobenius norm, and $j = \sqrt{-1}$.

II. MB-OFDM UWB OVERVIEW

A. WiMedia's MB-OFDM UWB PHY Specification

The structural diagram of the physical layer (PHY) of the WiMedia MB-OFDM UWB systems is shown in Fig. 1. WiMedia MB-OFDM UWB PHY specifications proposed by A. Batra et al. [1], [19] specify an UWB physical layer for a WPAN, utilizing the unlicensed 3.1 - 10.6 GHz frequency band, and supporting data rates of 53.3, 80, 106.7, 160, 200, 320, 400, and 480 Mb/s. The UWB spectrum is divided into 14 bands (see Fig. 2), each of which has a bandwidth of 528 MHz. The first 12 bands are then grouped into four band groups consisting of three bands, while the last two bands are grouped into the fifth band group. Support for the first band group is mandatory. A total of 100 data sub-carriers is used per band to transmit the information.

TABLE I
NUMBERS OF MULTIPATHS Np_{10dB} , $Np_{85\%}$, AND \bar{N}_p [15].

	CM 1	CM 2	CM 3	CM 4
Np_{10dB}	12.5	15.3	24.9	41.2
$Np_{85\%}$	20.8	33.9	64.7	123.3
\bar{N}_p	287.9	739.5	1463.7	3905.5

Frequency-domain spreading, time-domain spreading, and Forward Error Correction (FEC) coding are used to vary the data rates. The FEC used is a convolutional code with coding rates of 1/3, 1/2, 5/8 and 3/4. The coded binary data sequence then goes through a three-stage bit interleaver, consisting of symbol interleaver, tone interleaver, and cyclic shifter. The interleaved binary data sequence is then mapped into complex constellations. For data rates of 200 Mbps and lower, a QPSK constellation is used, while for the higher data rates, a multi-dimensional constellation using a DCM technique. This technique maps a group of four bits into two different 16-point constellations separated by 50 tones (sub-carriers) to better employ the frequency and time diversity [19].

The resulting data is inserted with 12 pilots and 10 guard sub-carriers, and is then transformed via the IFFT to form an OFDM symbol. The OFDM symbols are then padded with 37 zeros, which are considered as Zero-Padded Suffix (ZPS). ZPS is used to mitigate the effects of multi-path, and to provide a time window to allow the transmitter and receiver sufficient time to switch between the different frequencies. Most conventional wireless OFDM-based systems use a Cyclic Prefix (CP) to provide robustness against multipath. When a CP is used, redundancy or structure is introduced into the transmitted signal. This correlation in the transmitted signal causes ripples in the average Power Spectral Density (PSD), which, in MB-OFDM systems, could be as large as 1.5 dB [20]. Because the UWB emission is limited, the transmitted power must be reduced, resulting in a lower range for the system. When a ZPS is used, the ripples in the PSD can be reduced to zero, thus the power-backoff problem at the transmitter can be avoided, and the system can achieve the maximum possible range.

The coded data is then spread using a Time-Frequency Code (TFC) to achieve further time and frequency diversities. There are two types of TFCs: one where the coded information is interleaved over three bands, referred to as Time-Frequency Interleaving (TFI); and, one where the coded information is transmitted on a single band, referred to as Fixed Frequency Interleaving (FFI). Support for both TFI and FFI is mandatory.

B. IEEE 802.15.3a MB-OFDM UWB Channel Models

MB-OFDM UWB channel models proposed by Jeff Foerster et al. [15] are based on the Saleh-Valenzuela model with slight modification. The multipath gain magnitudes are modeled as independent log-normally distributed random variables (RVs) rather than Rayleigh variables, because the log-normally distributed variables fit better the measurement data. Independent fading is assumed for each cluster as well as each ray within the cluster. The discrete-time impulse response of the

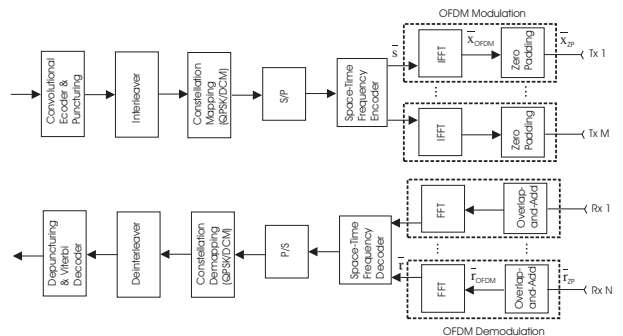


Fig. 3. Structural diagram of the proposed STFC MB-OFDM UWB systems.

multipath channel is

$$h_i(t) = X_i \sum_{l=0}^L \sum_{k=0}^K \alpha_{k,l}^i \delta(t - T_l^i - \tau_{k,l}^i) \quad (1)$$

where $\alpha_{k,l}^i$ are the multipath gain coefficients, T_l^i is the delay of the l -th cluster, $\tau_{k,l}^i$ is the delay of the k -th ray relative to the l -th cluster arrival time (T_l^i), X_i is the log-normal shadowing, and i is the index for the i -th realization.

The multipath gain coefficients are defined as

$$\alpha_{k,l} = p_{k,l} \xi_l \beta_{k,l} \quad (2)$$

where $p_{k,l}$ is equiprobable ± 1 to account for signal inversion due to reflection, ξ_l accounts for the fading relating to the l -th cluster, and $\beta_{k,l}$ reflects the fading relating to the k -th ray within the l -th cluster. $|\xi_l \beta_{k,l}|$ is modeled to be independent log-normally distributed RVs $|\xi_l \beta_{k,l}| = 10^{(\mu_{k,l} + n_1 + n_2)/20}$, where $\mu_{k,l}$ is the mean of the Gaussian RV $20 \log_{10}(|\xi_l \beta_{k,l}|)$ associated with the log-normal RV $|\xi_l \beta_{k,l}|$, n_1 and n_2 are independent Gaussian RVs with the distributions $\mathcal{N}(0, \sigma_1^2)$ and $\mathcal{N}(0, \sigma_2^2)$, relating to the fading on each cluster and ray, respectively. The value of $\mu_{k,l}$ can be found in [15].

There are four main IEEE MB-OFDM UWB channel models proposed by the IEEE 802.15.3a Task Group [15], accounting for the four typical multipath scenarios of UWB systems, namely CM 1 with a Light-Of-Sign (LOS) scenario and the distance between the transmitter and receiver is up to 4 m; CM 2 (Non Light-Of-Sign (NLOS), 0-4 m), CM 3 (NLOS, 4-10 m), and CM 4 proposed to fit the channel with the rms delay spread of 25 ns representing an extreme NLOS multipath channel. Denote Np_{10dB} , $Np_{85\%}$, and \bar{N}_p to be the number of multipaths arriving within 10 dB of the peak, the number of multipaths capturing 85% channel energy, and the average number of multipaths calculated over 100 channel realizations generated by the IEEE 802.15.3a UWB channel models [15]. The typical values of these parameters are shown in Table I. Clearly, UWB channels are very richly dispersive with the maximum number of resolvable multipaths reaching some thousands.

III. STFC MB-OFDM UWB SYSTEM

The diagram of the proposed STFC MB-OFDM UWB system with the notations of signals at the considered reference points is depicted in Fig. 3. The system consists of M Tx

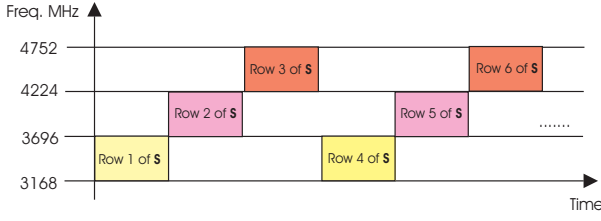


Fig. 4. An example of the transmitted RF pattern using the first band group.

antennas and N Rx antennas. We describe the transmitted STFC with the following matrix

$$\mathbf{S} = \{\bar{\mathbf{s}}_{t,m}\}_{T \times M}, \quad (3)$$

where T denotes the number of MB-OFDM symbol time slots required to transmit the whole STFC block. Structures of \mathbf{S} are the same as the structures of CO STBCs in conventional wireless STC MIMO systems [16], [18], [21], except that each element $\bar{\mathbf{s}}_{t,m}$ is not a complex number, but defined as a column vector $\bar{\mathbf{s}}_{t,m} = [s_{t,m,1}, s_{t,m,2}, \dots, s_{t,m,N_{fft}}]^T$. The vectors $\bar{\mathbf{s}}_{t,m}$ are the original transmitted data before IFFT. The symbols $s_{t,m,k}$ are drawn from a QPSK or DCM constellation.

Elements $\bar{\mathbf{s}}_{t,m}$ in each row of \mathbf{S} are transmitted simultaneously through M Tx antennas in the same frequency band, while different rows of \mathbf{S} might be transmitted in different frequency bands, following a certain TFC. An example of such TFCs is shown in Fig. 4.

Denote $\mathcal{X} = \{\bar{\mathbf{x}}_{OFDM,t,m}\}_{T \times M}$ to be the matrix whose elements are the N_{fft} -point IFFTs of the respective elements in \mathbf{S} , then

$$\mathcal{X} = \{IFFT\{\bar{\mathbf{s}}_{t,m}\}\}_{T \times M} = \{\bar{\mathbf{x}}_{OFDM,t,m}\}_{T \times M}. \quad (4)$$

The symbols $\bar{\mathbf{x}}_{OFDM,t,m}$ are referred to as MB-OFDM symbols. Further, denote with $\mathcal{X}_{ZP} = \{\bar{\mathbf{x}}_{ZP,t,m}\}_{T \times M}$ the matrix whose entries are the respective elements in \mathcal{X} appended by a ZPS of 37 zeros. Clearly, $\bar{\mathbf{x}}_{OFDM,t,m}$ is the transmitted MB-OFDM symbol before Zero Padding (ZP), while $\bar{\mathbf{x}}_{ZP,t,m}$ is the actual transmitted symbol after ZP. Denote

$$\bar{\mathbf{h}}_{m,n} = [h_{m,n,1}, h_{m,n,2}, \dots, h_{m,n,L_{m,n}}]^T \quad (5)$$

to be the channel vector between the m -th Tx and n -th Rx antennas, for $m = 1, \dots, M, n = 1, \dots, N$, where the channel coefficients $h_{m,n,l}$ of the l -th path, $l = 1, \dots, L_{m,n}$, in this channel are modeled as independent *log-normally* distributed RVs. Let $L_{max} = \max\{L_{m,n}\}$, for $m = 1, \dots, M, n = 1, \dots, N$. Denote the MB-OFDM UWB channel coefficient matrix as

$$\mathbf{H} = \{\bar{\mathbf{h}}_{m,n,ZP}\}_{M \times N} \quad (6)$$

where the vector $\bar{\mathbf{h}}_{m,n,ZP}$ is created from the corresponding channel vector $\bar{\mathbf{h}}_{m,n}$ by adding zeros to have the length L_{max} .

At the transmission of the t -th MB-OFDM symbol, the received signal at the n -th Rx antenna is calculated as

$$\bar{\mathbf{r}}_{ZP,t,n} = \sum_{m=1}^M (\bar{\mathbf{x}}_{ZP,t,m} \otimes \bar{\mathbf{h}}_{m,n}) + \bar{\mathbf{n}}_{t,n}. \quad (7)$$

The elements of noise vector $\bar{\mathbf{n}}_{t,n}$ are considered to be independent complex Gaussian RVs.

A. Theoretical Analysis

In this section, we first analyze the proposed system with the theoretical assumption that the maximum number of multipaths $L_{m,n}$, for $m = 1, \dots, M, n = 1, \dots, N$, is $(N_{ZPS} + 1)$, where N_{ZPS} denotes the length of the ZPS. As mentioned in Section II, instead of inserting a CP at the transmitter and discarding the CP at the receiver as in a conventional OFDM system, in an MB-OFDM system, a ZPS of a length N_{ZPS} is appended to each symbol $\bar{\mathbf{x}}_{OFDM,t,m}$ at the transmitter to create a transmitted symbol $\bar{\mathbf{x}}_{ZP,t,m}$. At the receiver, an Overlap-And-Add Operation (OAAO) must be performed before FFT. OAAO means that the N_{ZPS} samples of a received symbol $\bar{\mathbf{r}}_{ZP,t,n}$, ranging from $(N_{fft} + 1)$ to $(N_{fft} + N_{ZPS})$, are added to the beginning of that received symbol. Then the first N_{fft} samples of the resulting symbol will be used to decode the transmitted symbol. These N_{fft} samples are exactly equivalent to the *circular convolution* of the transmitted OFDM symbol (before ZP) $\bar{\mathbf{x}}_{OFDM,t,m}$ with the channel $\bar{\mathbf{h}}_{m,n}$. This exact equivalence is due to the fact that, if a ZPS of a length N_{ZPS} is used, the greatest multipath tolerance of the system is $(N_{ZPS} + 1)$. Consequently, from the theoretical viewpoint, the number of multipaths (the length of vectors $\bar{\mathbf{h}}_{m,n}$) must not exceed $(N_{ZPS} + 1)$.

As a result, after performing OAAO for the received signal $\bar{\mathbf{r}}_{ZP,t,n}$ in (7), and then taking the first N_{fft} resulting samples, denoted as $\bar{\mathbf{r}}_{OFDM,t,n}$, the following equation is deduced

$$\bar{\mathbf{r}}_{OFDM,t,n} = \sum_{m=1}^M \bar{\mathbf{x}}_{OFDM,t,m} * \bar{\mathbf{h}}_{m,n} + \bar{\mathbf{n}}_{t,n}. \quad (8)$$

For the circular convolution, we have the following property

$$\begin{aligned} \bar{\mathbf{x}}_{OFDM,t,m} * \bar{\mathbf{h}}_{m,n} &= IFFT\{FFT\{\bar{\mathbf{x}}_{OFDM,t,m}\} \bullet \\ &\quad FFT\{\bar{\mathbf{h}}_{m,n}\}\} \\ &= IFFT\{\bar{\mathbf{s}}_{t,m} \bullet \bar{\mathbf{h}}_{m,n}\} \end{aligned} \quad (9)$$

where $\bar{\mathbf{h}}_{m,n}$ is the N_{fft} -point FFT of the channel vector $\bar{\mathbf{h}}_{m,n}$, i.e.

$$\bar{\mathbf{h}}_{m,n} = FFT\{\bar{\mathbf{h}}_{m,n}\}. \quad (10)$$

We denote $\bar{\mathbf{h}}_{m,n} = [h_{m,n,1}, h_{m,n,2}, \dots, h_{m,n,N_{fft}}]^T$.

After going through the FFT block at the receiver, the received signal becomes

$$FFT\{\bar{\mathbf{r}}_{OFDM,t,n}\} = \sum_{m=1}^M \bar{\mathbf{s}}_{t,m} \bullet \bar{\mathbf{h}}_{m,n} + FFT\{\bar{\mathbf{n}}_{t,n}\} \quad (11)$$

Denote

$$\bar{\mathbf{v}}_{t,n} = [\mathbf{v}_{t,n,1}, \mathbf{v}_{t,n,2}, \dots, \mathbf{v}_{t,n,N_{fft}}]^T = FFT\{\bar{\mathbf{r}}_{OFDM,t,n}\}$$

and

$$\bar{\mathbf{n}}_{t,n} = [\mathbf{n}_{t,n,1}, \mathbf{n}_{t,n,2}, \dots, \mathbf{n}_{t,n,N_{fft}}]^T = FFT\{\bar{\mathbf{n}}_{t,n}\}.$$

Then (11) can be rewritten as follows

$$\bar{\mathbf{v}}_{t,n} = \sum_{m=1}^M \bar{\mathbf{s}}_{t,m} \bullet \bar{\mathbf{h}}_{m,n} + \bar{\mathbf{n}}_{t,n}. \quad (12)$$

Recall that $\bar{\mathbf{s}}_{t,n}$ is the original QPSK or DCM transmitted signal (before IFFT).

Denote $\mathcal{H} = \{\bar{\mathbf{h}}_{m,n}\}_{M \times N}$ to be the matrix whose elements are the N_{fft} -point FFTs of the respective elements in the channel-coefficient matrix \mathbf{H} . Further, denote $\mathbf{R} = \{\bar{\mathbf{r}}_{OFDM,t,n}\}_{T \times N}$ to be the received signal matrix, $\mathcal{R} = \{\bar{\mathbf{r}}_{t,n}\}_{T \times N}$ to be the received signal matrix after FFT, and $\mathcal{N} = \{\bar{\mathbf{n}}_{t,n}\}_{T \times N}$ to be a noise matrix. We can rewrite (12) in matrix form as follows

$$\mathcal{R} = \mathbf{S} \circ \mathcal{H} + \mathcal{N}. \quad (13)$$

From (13), we can realize that there exists a similarity between the mathematical model of the STFC MB-OFDM UWB system and that of the conventional wireless STC MIMO system [16], [18], [22]. The only difference between the two mathematical models is that the matrix elements are scalar numbers in the conventional STC MIMO system, while they are N_{fft} -length vectors in the STFC MB-OFDM UWB system.

Because the vector elements in \mathbf{S} will be transformed with the IFFT to generate MB-OFDM symbols with N_{fft} subcarriers, we refer to \mathbf{S} as a Space-Time-Frequency Code.

B. Realistic Channel Condition

The error performance of the proposed system with realistic UWB channel conditions is inferior, compared to the theoretical performance, due to the following two main reasons.

In theory, the length of CP or ZPS must be longer than the longest multipath in an OFDM-based system to turn the linear convolution between the transmitted signal and the channel vector into the circular convolution. However, in practice, the multipath length is very likely to exceed the length of CP or ZPS. This is especially true in MB-OFDM UWB systems where the average number of multipaths \bar{N}_p is usually much bigger than $N_{ZPS} = 37$ (see Table I). The transition from (7) to (12) is an approximation, due to the fact that the circular convolution in (9) is approximate, but not exactly equal to the first N_{fft} samples achieved by the OAAO of the linear convolution $\bar{\mathbf{x}}_{ZP,t,m} \otimes \bar{\mathbf{h}}_{m,n}$ in (7). The energy of multipath components within the ZPS window will be captured, while the multipath components outside this window may be considered as interferences for the received signals. Eq. (7) represents the real received signals at the Rx antennas, while (12) shows the realistic concept used at the STFC decoder to decode the original transmitted signals. Therefore, in order to simulate the realistic performance of the proposed system, the signals received at the Rx antennas should be calculated from (7) with the linear convolution between the transmitted MB-OFDM symbols and the fully long multipath channels, while decoding algorithm should be carried out based on (12), i.e. based on the circular convolution.

On the other hand, for a channel vector $\bar{\mathbf{h}}_{m,n} = [h_{m,n,1}, h_{m,n,2}, \dots, h_{m,n,L_{m,n}}]^T$, we always have the following property for the N_{fft} -point FFT operation

$$FFT\{\bar{\mathbf{h}}_{m,n}\} = FFT\{[h_{m,n,1}, h_{m,n,2}, \dots, h_{m,n,L_{m,n}}]^T\}$$

if the length $L_{m,n}$ of the vector is not smaller than N_{fft} . This means that, by FFT-ing the received signals with a *limited*

FFT size N_{fft} , and decoding signals based on (12), the N_{fft} -point FFT operation truncates the impact of a long vector $\bar{\mathbf{h}}_{m,n}$ to the length of N_{fft} . Therefore, the higher N_{fft} is, the closer the approximation between the linear convolution and the circular convolution is, and thus the better the system performance is. However, FFT and IFFT blocks significantly decide the complexity and the cost of transmitter and receiver. As a result, there must be a suitable compromise between the cost/complexity and the system performance.

IV. PAIRWISE ERROR PROBABILITY

Due to the similarity between the mathematical model of the STFC MB-OFDM system and that of the conventional wireless STC MIMO system as shown in (13), we can calculate the PEP of the proposed STFC MB-OFDM system, based on Tarokh's method mentioned in [5] for conventional wireless STC MIMO communications, with proper modifications to account for the MB-OFDM UWB channels. We consider a STFC MB-OFDM MIMO system with M Tx, N Rx antennas, and with the STFC \mathbf{S} defined in (3). We denote E_s to be the average energy of the signal constellation. The following analysis is derived without considering a specific modulation scheme, thus can be applied to different modulation schemes.

We consider the probability that a ML receiver decides erroneously in favor of a signal

$$\mathbf{e} = [e_{1,1,1} \dots e_{1,1,N_{fft}}, e_{1,2,1} \dots e_{1,2,N_{fft}}, \dots, e_{T,M,1} \dots e_{T,M,N_{fft}}] \quad (14)$$

assuming that

$$\mathbf{c} = [c_{1,1,1} \dots c_{1,1,N_{fft}}, c_{1,2,1} \dots c_{1,2,N_{fft}}, \dots, c_{T,M,1} \dots c_{T,M,N_{fft}}] \quad (15)$$

was transmitted. Note that each group of N_{fft} consecutive data inside \mathbf{c} in fact form a certain vector $\bar{\mathbf{s}}$ as defined in (3).

If the transmission coefficients are known at the receiver, the probability of transmitting \mathbf{c} and deciding \mathbf{e} at the decoder is well approximated by the Chernoff bound

$$P(\mathbf{c} \rightarrow \mathbf{e} | \bar{\mathbf{h}}_{m,n,k}, m = 1, \dots, M; n = 1, \dots, N; k = 1, \dots, N_{fft}) \leq \exp(-d^2(\mathbf{c}, \mathbf{e})E_s/4N_0) \quad (16)$$

where $N_0/2$ is the noise variance per dimension and

$$d^2(\mathbf{c}, \mathbf{e}) = \sum_{n=1}^N \sum_{t=1}^T \sum_{k=1}^{N_{fft}} \left| \sum_{m=1}^M \bar{h}_{m,n,k} (c_{t,m,k} - e_{t,m,k}) \right|^2. \quad (17)$$

Setting $\Omega_{n,k} = (\bar{h}_{1,n,k}, \dots, \bar{h}_{M,n,k})$ for $n = 1, \dots, N, k = 1, \dots, N_{fft}$, we rewrite (17) as

$$d^2(\mathbf{c}, \mathbf{e}) = \sum_{n=1}^N \sum_{k=1}^{N_{fft}} \sum_{m=1}^M \sum_{\hat{m}=1}^M [\bar{h}_{m,n,k} \bar{h}_{\hat{m},n,k}^* \sum_{t=1}^T (c_{t,m,k} - e_{t,m,k})(c_{t,\hat{m},k} - e_{t,\hat{m},k})^*] \quad (18)$$

With the square, order- M matrix $\mathbf{A}_k(\mathbf{c}, \mathbf{e}) = \{A_{p,q,k}\}$, where

$$A_{p,q,k} = \sum_{t=1}^T (c_{t,p,k} - e_{t,p,k})(c_{t,q,k} - e_{t,q,k})^* \quad (19)$$

for $p, q = 1, \dots, M$, Eq. (18) becomes

$$d^2(\mathbf{c}, \mathbf{e}) = \sum_{n=1}^N \sum_{k=1}^{N_{fft}} \Omega_{n,k} \mathbf{A}_k(\mathbf{c}, \mathbf{e}) \Omega_{n,k}^H. \quad (20)$$

It is clear that $\mathbf{A}_k(\mathbf{c}, \mathbf{e})$ is Hermitian, i.e. $\mathbf{A}_k(\mathbf{c}, \mathbf{e}) = \mathbf{A}_k(\mathbf{c}, \mathbf{e})^H$. Hence, there exists a unitary matrix \mathbf{V}_k and a real diagonal matrix \mathbf{D}_k such that $\mathbf{V}_k \mathbf{A}_k \mathbf{V}_k^H = \mathbf{D}_k$. The diagonal elements of \mathbf{D}_k are the eigenvalues $\lambda_{m,k}$, for $m = 1, \dots, M$, and $k = 1, \dots, N_{fft}$, of $\mathbf{A}_k(\mathbf{c}, \mathbf{e})$. By construction, the matrix

$$\mathbf{B}_k(\mathbf{c}, \mathbf{e}) = \begin{bmatrix} c_{1,1,k} - e_{1,1,k} & \dots & c_{1,M,k} - e_{1,M,k} \\ c_{2,1,k} - e_{2,1,k} & \dots & c_{2,M,k} - e_{2,M,k} \\ \dots & \dots & \dots \\ c_{T,1,k} - e_{T,1,k} & \dots & c_{T,M,k} - e_{T,M,k} \end{bmatrix} \quad (21)$$

is clearly a square root of $\mathbf{A}_k(\mathbf{c}, \mathbf{e})$, i.e. $\mathbf{B}_k(\mathbf{c}, \mathbf{e})^H \mathbf{B}_k(\mathbf{c}, \mathbf{e}) = \mathbf{A}_k(\mathbf{c}, \mathbf{e})$. Therefore, the eigenvalues $\lambda_{m,k}$ of $\mathbf{A}_k(\mathbf{c}, \mathbf{e})$ are nonnegative real numbers. It is noted that $\mathbf{B}_k(\mathbf{c}, \mathbf{e})$ can be created from the STFC matrix \mathbf{S} in (3) by replacing each vector element of \mathbf{S} with the non-vector term $(c_{m,n,k} - e_{m,n,k})$.

Let

$$(\beta_{1,n,k}, \beta_{2,n,k}, \dots, \beta_{M,n,k}) = \Omega_{n,k} \mathbf{V}_k^H \quad (22)$$

we have

$$\Omega_{n,k} \mathbf{A}_k(\mathbf{c}, \mathbf{e}) \Omega_{n,k}^H = \sum_{m=1}^M \lambda_{m,k} |\beta_{m,n,k}|^2. \quad (23)$$

As mentioned in Section II, the magnitudes of the channel coefficients $h_{m,n,l}$, for $m = 1, \dots, M$, $n = 1, \dots, N$, and $l = 1, \dots, L_{m,n}$, are independent, *log-normally distributed* (rather than Rayleigh distributed) RVs (*not necessary identical*). It is known that if $Y = \sum_{i=1}^J X_i$, where J is a finite number and X_i are the independent log-normally distributed RVs with the distribution $\text{Log-N}(\mu_i, \sigma_i^2)$, then the distribution of Y has no available closed-form expression, but can be reasonably well approximated by another log-normally distributed RV $Z \sim \text{Log-N}(\mu_Z, \sigma_Z^2)$, for instance, using the Fenton-Wilkinson approximation [23] with the following distribution parameters

$$\sigma_Z^2 = \ln \left[1 + \frac{\sum_{i=1}^J e^{2\mu_i + \sigma_i^2} (e^{\sigma_i^2} - 1)}{(\sum_{i=1}^J e^{\mu_i + \sigma_i^2/2})^2} \right]$$

$$\mu_Z = \ln \left(\sum_{i=1}^J e^{\mu_i + \sigma_i^2/2} \right) - \frac{\sigma_Z^2}{2}$$

Note that, because J is a finite number, the central-limit theorem cannot be applied in this case. Also, the distribution parameters of a log-normally distributed RV x should be understood to be the mean and variance of the normally (Gaussian) distributed RV associated with x .

Expanding this property for the case

$$Y = \sum_{i=1}^J p_i e^{a_i} X_i \quad (24)$$

where a_i are real or complex numbers, and $p_i = \pm 1$, based on Eqs. (15)–(17) in [23] and with simple manipulations, we can deduce the distribution parameters of the approximate log-normally distributed RV Z as follows

$$\sigma_Z^2 = \ln \left[1 + \frac{\sum_{i=1}^J p_i^2 e^{2\eta_i + \sigma_i^2} (e^{\sigma_i^2} - 1)}{(\sum_{i=1}^J p_i e^{\eta_i + \sigma_i^2/2})^2} \right]$$

$$\mu_Z = \ln \left(\sum_{i=1}^J p_i e^{\eta_i + \sigma_i^2/2} \right) - \frac{\sigma_Z^2}{2} \quad (25)$$

where $\eta_i = \mu_i + a_i$.

Since the average number of multipaths of UWB channels \bar{N}_p is much higher than N_{fft} (see Table I), the elements $\bar{h}_{m,n,k}$ of the channel vector $\bar{\mathbf{h}}_{m,n}$, which is the N_{fft} -point FFT of the channel vector $\bar{\mathbf{h}}_{m,n}$, can be represented as

$$\bar{h}_{m,n,k} = \sum_{l=1}^{N_{fft}} h_{m,n,l} e^{-\frac{j2\pi(l-1)(k-1)}{N_{fft}}}. \quad (26)$$

The multipath components $h_{m,n,l}$ defined in (1) are *real* numbers with equiprobable negative and positive values representing the signal inversion due to reflections. Thus we write $h_{m,n,l} = \pm |h_{m,n,l}|$. Further, the magnitudes $|h_{m,n,l}|$ of multipath components are independent log-normally distributed RVs. Denote $Eh_{m,n,l}$ and $\theta_{m,n,l}^2$ to be the mean and variances of the normally distributed RV associated with the log-normally distributed RV $|h_{m,n,l}|$. Thus, $|h_{m,n,l}|$ follow the log-normal distribution $\text{Log-N}(Eh_{m,n,l}, \theta_{m,n,l}^2)$. To quantify the distribution parameters of $\bar{h}_{m,n,k}$, we rewrite (26) as

$$\bar{h}_{m,n,k} = \sum_{l=1}^{N_{fft}} p_{m,n,l} |h_{m,n,l}| e^{-\frac{j2\pi(l-1)(k-1)}{N_{fft}}} \quad (27)$$

where $p_{m,n,l} = \pm 1$ depending on whether $h_{m,n,l}$ is positive or negative. Clearly, (27) is in the similar form as (24). Therefore, $\bar{h}_{m,n,k}$ can be approximated by a *complex* log-normally distributed RV $Z_{m,n,k}$. From (25), the distribution parameters of $Z_{m,n,k}$ are derived as follows

$$\sigma_{Z_{m,n,k}}^2 = \ln \left[1 + \frac{\sum_{l=1}^{N_{fft}} e^{2\eta_{m,n,k,l} + \theta_{m,n,l}^2} (e^{\theta_{m,n,l}^2} - 1)}{(\sum_{l=1}^{N_{fft}} p_{m,n,l} e^{\eta_{m,n,k,l} + \theta_{m,n,l}^2/2})^2} \right]$$

$$\mu_{Z_{m,n,k}} = \ln \left(\sum_{l=1}^{N_{fft}} p_{m,n,l} e^{\eta_{m,n,k,l} + \theta_{m,n,l}^2/2} \right) - \frac{\sigma_{Z_{m,n,k}}^2}{2} \quad (28)$$

where $\eta_{m,n,k,l} = Eh_{m,n,l} - \frac{j2\pi(l-1)(k-1)}{N_{fft}}$.

From the mutual relation between the mean and variance of a log-normally distributed RV and the normally distributed RV associated with it [17], we can quantify the mean and variance of $\bar{h}_{m,n,k}$, denoted as $E\bar{h}_{m,n,k}$ and $\varrho_{m,n,k}^2$ respectively, as follows

$$E\bar{h}_{m,n,k} = e^{\mu_{Z_{m,n,k}} + \sigma_{Z_{m,n,k}}^2/2}$$

$$\varrho_{m,n,k}^2 = (e^{\sigma_{Z_{m,n,k}}^2} - 1) e^{2\mu_{Z_{m,n,k}} + \sigma_{Z_{m,n,k}}^2} \quad (29)$$

As a result, the N_{fft} -point FFT of a channel vector $\bar{\mathbf{h}}_{m,n}$ consisting of $L_{m,n}$ ($L_{m,n} > N_{fft}$) real multipath components $h_{m,n,l}$ (for $l = 1, \dots, L_{m,n}$), whose magnitudes are

independent log-normally distributed RVs, produces a channel vector $\bar{\mathbf{h}}_{m,n}$ consisting of N_{fft} complex multipath components $\bar{h}_{m,n,k}$ (for $k = 1, \dots, N_{fft}$), which are *independent* log-normally distributed RVs. It should be emphasized that, from the mathematical viewpoint, if the FFT size N_{fft} is not smaller than the average number of multipath components \bar{N}_p , which is usually not the case of MB-OFDM UWB systems, then the N_{fft} -point FFT of $\bar{\mathbf{h}}_{m,n}$ produces a vector $\bar{\mathbf{h}}_{m,n}$ consisting of \bar{N}_p (rather than N_{fft}) *independent* log-normally distributed RVs.

Since \mathbf{V}_k is unitary, the rows $\{v_{1,k}, v_{2,k}, \dots, v_{M,k}\}$ of \mathbf{V}_k are a complete orthonormal basis of the complex M -dimensional space \mathcal{C}^M , and thus, from (22) and the general property (24) of a sum of independent log-normally distributed RVs, $\beta_{m,n,k}$ (for $m = 1, \dots, M$, $n = 1, \dots, N$ and $k = 1, \dots, N_{fft}$) can also be reasonably well approximated to be complex, *independent* log-normally distributed RVs. Note that if $\beta_{m,n,k}$ is a *complex* log-normally distributed RV, then $|\beta_{m,n,k}|$ is a *real* log-normally distributed RV. That is because we can always represent $\beta_{m,n,k}$ in the form $\beta_{m,n,k} = e^\omega = e^{\omega_R + j\omega_I}$, where ω_R and ω_I are the real and imaginary parts of the complex, normally distributed RV ω . Therefore, $|\beta_{m,n,k}| = e^{\omega_R}$ is a real, log-normally distributed RV with the associated normally distributed RV ω_R .

Denote the mean and variance of $|\beta_{m,n,k}|$ as $E_{m,n,k}$ and $\gamma_{m,n,k}^2$ respectively, then $|\beta_{m,n,k}|$ are independent log-normally distributed RVs with the following pdf

$$p(|\beta_{m,n,k}|) = \frac{1}{|\beta_{m,n,k}| \sigma_{m,n,k} \sqrt{2\pi}} \exp \left[-(\ln(|\beta_{m,n,k}|) - \mu_{m,n,k})^2 / (2\sigma_{m,n,k}^2) \right] \quad (30)$$

where

$$\begin{aligned} \mu_{m,n,k} &= \ln(E_{m,n,k}) - \frac{1}{2} \ln \left(1 + \frac{\gamma_{m,n,k}^2}{E_{m,n,k}^2} \right) \\ \sigma_{m,n,k}^2 &= \ln \left(1 + \frac{\gamma_{m,n,k}^2}{E_{m,n,k}^2} \right). \end{aligned} \quad (31)$$

Denote $K_{m,n,k}$ to be the mean of $|\beta_{m,n,k}|^2$. Thus $K_{m,n,k}$ is the second moment of $|\beta_{m,n,k}|$, and therefore [17]

$$K_{m,n,k} = e^{(2\mu_{m,n,k} + 2\sigma_{m,n,k}^2)} \quad (32)$$

If $|\beta_{m,n,k}|$ is a log-normally distributed RV, so is $|\beta_{m,n,k}|^2$. From (16), (20), and (23), to compute the upper bound on the average probability of error, we simply average

$$\exp \left[- (E_s/4N_0) \sum_{n=1}^N \sum_{k=1}^{N_{fft}} \sum_{m=1}^M \lambda_{m,n,k} |\beta_{m,n,k}|^2 \right] \quad (33)$$

with respect to independent log-normal distribution of $|\beta_{m,n,k}|^2$. We denote $\Xi_{m,n,k} = |\beta_{m,n,k}|^2$.

It is noted that, if $\Xi_{m,n,k}$ is a log-normally distributed RV (i.e. $\Xi_{m,n,k} = e^y$ where $y \sim \mathcal{N}(\mu, \sigma^2)$, and μ, σ^2 are finite numbers) and α is a positive coefficient, it is possible to prove that $E\{e^{-\alpha\Xi_{m,n,k}}\} \leq \frac{1}{\alpha} e^{-E\{\Xi_{m,n,k}\}}$ for a sufficient large α , i.e. $\alpha \geq \alpha_0$ (see Appendix I). Therefore, if a sufficiently large

signal-to-noise ratio E_s/N_0 is considered, we have

$$P(\mathbf{c} \rightarrow \mathbf{e}) \leq \left[(E_s/4N_0)^{-rNN_{fft}} \left(\prod_{k=1}^{N_{fft}} \prod_{m=1}^r \lambda_{m,k} \right)^{-N} \prod_{n=1}^N \prod_{k=1}^{N_{fft}} \prod_{m=1}^r \exp(-K_{m,n,k}) \right] \quad (34)$$

where $r = \min\{r_k\}$, and r_k , for $k = 1, \dots, N_{fft}$, is the rank of matrix $\mathbf{B}_k(\mathbf{c}, \mathbf{e})$.

We realize that a diversity order of rNN_{fft} and a coding gain (over MB-OFDM systems without STFCs) of

$$\begin{aligned} & \left(\prod_{k=1}^{N_{fft}} \prod_{m=1}^r \lambda_{m,k} \right)^{1/rNN_{fft}} \times \\ & \left[\prod_{n=1}^N \prod_{k=1}^{N_{fft}} \prod_{m=1}^r \exp(-K_{m,n,k}) \right]^{-1/rNN_{fft}} \end{aligned} \quad (35)$$

are achieved. Therefore, the maximum achievable diversity order in STFC MB-OFDM UWB systems is the product between number of Tx antennas, the number of Rx antennas, and the FFT size.

We note that the maximum diversity order is defined here as the maximum diversity order of the outgoing signals from the OFDM demodulation block in Fig. 1, which are evaluated by (12). The maximum diversity order of the incoming signals received at Rx antennas (before the OFDM demodulation block, calculated by (7)) may be very large due to the very dispersive multipath channel, while the maximum diversity order of the outgoing signals from the OFDM demodulation block is limited because the FFT size is normally very limited, compared to the full length of multipaths. Thus the maximum diversity order of the outgoing signals from the OFDM demodulation block should be considered, rather than the incoming signals. The former represents the effect of an important technical specification of the system, i.e. the FFT size of the OFDM demodulation block, while the latter does not.

It is interesting that the diversity order achieved by our approach agrees with that mentioned in Eq. (23) of the independent work [12], provided we consider the case where the average number of multipaths is in fact higher than the FFT size. However, the authors in [12] misjudged this fact, thus came to the conclusion that the maximum achievable diversity order is the product between the number of Tx antennas, the number of Rx antennas, the number of multipath components, and the number of jointly encoded OFDM symbols. Furthermore, our PEP formulation is carried out directly for the case of log-normal distribution of UWB channel magnitudes, which has not been examined in [12]. Our PEP is formulated without assumptions on the same time delays and the same average power of all transmit-receive links as in [12]. Additionally, the approach in [12] does not reflect clearly the essence of the effect of the FFT operation to the diversity order. In contrast, our approach shows clearly that the FFT size actually decides the number of *independent* log-normally distributed RVs $|\beta_{m,n,k}|$, that in turn decides the diversity order. If the FFT size N_{fft} is not smaller than the average number \bar{N}_p

TABLE II

DECODING METRICS FOR \mathbf{S}_2 WITH PSK OR QAM MODULATIONS.

Symbol	Decoding Metric
\bar{s}_1	$\arg \min_{\bar{s} \in \mathcal{C}^{ND}} \left\ \left[\left(\bar{h}_1^* \bullet \bar{c}_1 + \bar{h}_2 \bullet \bar{c}_2^* \right) - \bar{s} \right] \cdot \wedge 2 + \left(-\bar{1} + \sum_{m=1}^2 \bar{h}_m \cdot \wedge 2 \right) \bullet \left(\bar{s} \cdot \wedge 2 \right) \right\ _F^2$
\bar{s}_2	$\arg \min_{\bar{s} \in \mathcal{C}^{ND}} \left\ \left[\left(\bar{h}_2^* \bullet \bar{c}_1 - \bar{h}_1 \bullet \bar{c}_2^* \right) - \bar{s} \right] \cdot \wedge 2 + \left(-\bar{1} + \sum_{m=1}^2 \bar{h}_m \cdot \wedge 2 \right) \bullet \left(\bar{s} \cdot \wedge 2 \right) \right\ _F^2$

of multipath components, then N_{fft} in (34) must be replaced with \bar{N}_p , because there are only \bar{N}_p independent RVs among N_{fft} variables $|\beta_{m,n,k}|$, for certain numbers m and n , thus the maximum diversity order is $MN\bar{N}_p$. However, this is usually *not* the case for MB-OFDM UWB channels due to the fact that UWB channels are richly dispersive, while the FFT size is limited. Finally, our approach also clearly shows that, within a range up to \bar{N}_p , the higher the FFT size is, the lower the error bound in (34) is. This agrees with the analysis mentioned previously in Section III-B.

V. DESIGN CRITERIA FOR STFCs IN MB-OFDM UWB

Assuming that all the multipath components are known at the receiver. From (34), we derive the following design criteria of STFCs in MB-OFDM UWB systems for a large SNR to minimize the upper bound of error probability

- Diversity Gain Criterion: In order to achieve the maximum diversity order of MNN_{fft} , the *minimum* rank of matrices $\mathbf{B}_k(\mathbf{c}, \mathbf{e})$, for $k = 1, \dots, N_{fft}$, over any two distinct code words \mathbf{c} and \mathbf{e} must be equal to M . If the minimum rank is r , then a diversity of rNN_{fft} is achieved.
- Coding Gain Criterion: Suppose that a diversity of order rNN_{fft} is of our interest. The minimum of the product

$$\left(\prod_{k=1}^{N_{fft}} \prod_{m=1}^r \lambda_{m,k} \right)^{1/rN_{fft}} \times \left[\prod_{n=1}^N \prod_{k=1}^{N_{fft}} \prod_{m=1}^r \exp(-K_{m,n,k}) \right]^{-1/rN_{fft}}$$

taken over distinct codewords \mathbf{c} and \mathbf{e} has to be maximized.

Interestingly, all CO STBCs proposed in the literature for conventional STBC MIMO systems can satisfy the diversity gain criterion. This is because, a CO STBC S transmitted through a wireless system with M Tx antennas during T time slots can be defined [18], [24] as a $T \times M$ -size matrix whose nonzero entries are the indeterminates s_1, s_2, \dots, s_k , their conjugates $s_1^*, s_2^*, \dots, s_k^*$, or their products with $j = \sqrt{-1}$ over the complex number field \mathcal{C} , such that

$$S^H S = D \quad (36)$$

where D is a diagonal matrix of size $M \times M$ with diagonal entries $D_{i,i}$, for $i = 1, 2, \dots, M$, of the form $(l_{i,1}|s_1|^2 + l_{i,2}|s_2|^2 + \dots + l_{i,k}|s_k|^2)$. The coefficients $l_{i,k}$ are strictly

TABLE III

DECODING METRICS FOR \mathbf{S}_8 WITH PSK OR QAM MODULATIONS.

Symbol	Decoding Metric
\bar{s}_1	$\arg \min_{\bar{s} \in \mathcal{C}^{ND}} \left\ \left[\left(\bar{h}_3^* \bullet \bar{c}_7 + \bar{h}_6^* \bullet \bar{c}_5 + \bar{h}_7^* \bullet \bar{c}_7 + \bar{h}_3^* \bullet \bar{c}_3 + \bar{h}_1^* \bullet \bar{c}_1 + \bar{h}_6 \bullet \bar{c}_6^* + \bar{h}_5^* \bullet \bar{c}_1 - \bar{h}_5 \bullet \bar{c}_3^* + \bar{h}_2 \bullet \bar{c}_2^* - \bar{h}_1 \bullet \bar{c}_2^* + \bar{h}_5^* \bullet \bar{c}_5 + \bar{h}_4^* \bullet \bar{c}_3 - \bar{h}_3 \bullet \bar{c}_4^* + \bar{h}_4 \bullet \bar{c}_4^* - \bar{h}_7 \bullet \bar{c}_8^* + \bar{h}_8 \bullet \bar{c}_8^* \right) - \bar{s} \right] \cdot \wedge 2 + \left(-\bar{1} + 2 \sum_{m=1}^8 \bar{h}_m \cdot \wedge 2 \right) \bullet \left(\bar{s} \cdot \wedge 2 \right) \right\ _F^2$
\bar{s}_2	$\arg \min_{\bar{s} \in \mathcal{C}^{ND}} \left\ \left[\left(-\bar{h}_5 \bullet \bar{c}_8^* + \bar{h}_8 \bullet \bar{c}_6^* + \bar{h}_7 \bullet \bar{c}_6^* - \bar{h}_3 \bullet \bar{c}_1^* + \bar{h}_4 \bullet \bar{c}_1^* - \bar{h}_7^* \bullet \bar{c}_5 - \bar{h}_6^* \bullet \bar{c}_7 + \bar{h}_1 \bullet \bar{c}_3^* + \bar{h}_3^* \bullet \bar{c}_2 + \bar{h}_4^* \bullet \bar{c}_2 - \bar{h}_2 \bullet \bar{c}_3^* + \bar{h}_8^* \bullet \bar{c}_5 - \bar{h}_1^* \bullet \bar{c}_4 - \bar{h}_2^* \bullet \bar{c}_4 + \bar{h}_5^* \bullet \bar{c}_7 - \bar{h}_6 \bullet \bar{c}_8^* \right) - \bar{s} \right] \cdot \wedge 2 + \left(-\bar{1} + 2 \sum_{m=1}^8 \bar{h}_m \cdot \wedge 2 \right) \bullet \left(\bar{s} \cdot \wedge 2 \right) \right\ _F^2$
\bar{s}_3	$\arg \min_{\bar{s} \in \mathcal{C}^{ND}} \left\ \left[\left(-\bar{h}_1^* \bullet \bar{c}_6 - \bar{h}_2^* \bullet \bar{c}_6 - \bar{h}_5 \bullet \bar{c}_1^* + \bar{h}_6 \bullet \bar{c}_1^* - \bar{h}_2 \bullet \bar{c}_5^* - \bar{h}_8 \bullet \bar{c}_4^* + \bar{h}_1 \bullet \bar{c}_5^* + \bar{h}_5^* \bullet \bar{c}_2 + \bar{h}_7^* \bullet \bar{c}_3 + \bar{h}_6^* \bullet \bar{c}_2 - \bar{h}_3^* \bullet \bar{c}_7 - \bar{h}_8^* \bullet \bar{c}_3 - \bar{h}_7 \bullet \bar{c}_4^* + \bar{h}_4^* \bullet \bar{c}_7 + \bar{h}_3 \bullet \bar{c}_8^* + \bar{h}_4 \bullet \bar{c}_8^* \right) - \bar{s} \right] \cdot \wedge 2 + \left(-\bar{1} + 2 \sum_{m=1}^8 \bar{h}_m \cdot \wedge 2 \right) \bullet \left(\bar{s} \cdot \wedge 2 \right) \right\ _F^2$
\bar{s}_4	$\arg \min_{\bar{s} \in \mathcal{C}^{ND}} \left\ \left[\left(\bar{h}_7^* \bullet \bar{c}_2 - \bar{h}_2 \bullet \bar{c}_7^* - \bar{h}_1^* \bullet \bar{c}_8 - \bar{h}_2^* \bullet \bar{c}_8 + \bar{h}_3^* \bullet \bar{c}_5 - \bar{h}_7 \bullet \bar{c}_1^* + \bar{h}_8 \bullet \bar{c}_1^* - \bar{h}_5^* \bullet \bar{c}_3 + \bar{h}_6^* \bullet \bar{c}_3 + \bar{h}_1 \bullet \bar{c}_2^* + \bar{h}_8^* \bullet \bar{c}_2 - \bar{h}_4^* \bullet \bar{c}_5 + \bar{h}_5 \bullet \bar{c}_4^* + \bar{h}_6 \bullet \bar{c}_4^* - \bar{h}_3 \bullet \bar{c}_6^* - \bar{h}_4 \bullet \bar{c}_6^* \right) - \bar{s} \right] \cdot \wedge 2 + \left(-\bar{1} + 2 \sum_{m=1}^8 \bar{h}_m \cdot \wedge 2 \right) \bullet \left(\bar{s} \cdot \wedge 2 \right) \right\ _F^2$

positive, real numbers. Since the time delay for transmitting the CO STBC T is at least equal to M , from (36), the rank of S is always equal to M . Therefore, if the structures of conventional CO STBCs are used to create STFCs in MB-OFDM UWB systems, the diversity gain criterion is always guaranteed. In other words, from the diversity viewpoint, the design criteria are the same for both conventional STBC MIMO system and STFC MB-OFDM UWB system.

As an example, the Alamouti code [16] for two Tx antennas is a STFC providing a full diversity of $2NN_{fft}$ for any two distinct codewords \mathbf{c} and \mathbf{e} . Our proposed codes in [18] for 8 Tx antennas are some examples, among various other examples of STFCs for 8 Tx antennas, providing a full diversity order of $8NN_{fft}$, for any distinct codewords \mathbf{c} and \mathbf{e} .

VI. MAXIMUM LIKELIHOOD DECODING ALGORITHM

From (13), the ML decoding expression can be derived in the most general form as follows

$$\{\bar{s}_{dec,t,m}\} = \arg \min_{\{\bar{s}_{t,m}\}} \left\| \mathcal{R} - \mathbf{S} \circ \mathcal{H} \right\|_F^2. \quad (37)$$

This decoding metric is too complicated to be performed if \mathbf{S} has non-orthogonal structures. Fortunately, because \mathbf{S} has the similar structures as the conventional CO STBCs, the orthogonality of \mathbf{S} is preserved for the MB-OFDM symbols $\bar{s}_{t,m}$ transmitted inside the code block \mathbf{S} . As a result, the simplicity of decoding CO STBCs in conventional wireless STBC MIMO systems is also preserved in STFC MB-OFDM UWB systems, i.e., each MB-OFDM symbol $\bar{s}_{t,m}$ can be

decoded separately, rather than jointly. Therefore, decoding metrics for the MB-OFDM symbols $\bar{s}_{t,m}$ can be easily found, based on those decoding metrics for the respective CO STBC of \mathbf{S} , with slight modifications. Furthermore, each data point among N_D data points ($N_D = 100$ data sub-carriers) within a MB-OFDM symbol $\bar{s}_{t,m}$ can also be decoded separately, rather than the whole N_D data in a MB-OFDM symbol $\bar{s}_{t,m}$ are decoded simultaneously. Thus the decoding process is completely linear, and relatively simple.

According to the WiMedia's MB-OFDM UWB specifications, the convolutional encoder is utilized at the transmitter. Therefore, the transmitted binary information will be recovered at the receiver by using a Viterbi decoder, after all of the signals at the FFT points are separately decoded as mentioned above.

To illustrate the ML decoding algorithm for STFCs implemented in MB-OFDM UWB systems, we consider here two CO STBCs: the Alamouti code for two Tx antennas

$$\mathbf{S}_2 = \begin{bmatrix} \bar{s}_1 & \bar{s}_2 \\ -\bar{s}_2^* & \bar{s}_1^* \end{bmatrix} \quad (38)$$

and the code proposed in [18] for 8 Tx antennas

$$\mathbf{S}_8 = \begin{bmatrix} \bar{s}_1 & \bar{s}_1 & -\bar{s}_2^* & \bar{s}_2^* & -\bar{s}_3^* & \bar{s}_3^* & -\bar{s}_4^* & \bar{s}_4^* \\ -\bar{s}_1^* & \bar{s}_1^* & \bar{s}_2 & \bar{s}_2 & \bar{s}_3 & \bar{s}_3 & \bar{s}_4 & \bar{s}_4 \\ \bar{s}_2^* & -\bar{s}_2^* & \bar{s}_1 & \bar{s}_1 & -\bar{s}_4 & \bar{s}_4 & \bar{s}_3 & -\bar{s}_3 \\ -\bar{s}_2 & -\bar{s}_2 & -\bar{s}_1^* & \bar{s}_1^* & \bar{s}_4^* & \bar{s}_4^* & -\bar{s}_3^* & -\bar{s}_3^* \\ \bar{s}_3^* & -\bar{s}_3^* & \bar{s}_4 & -\bar{s}_4 & \bar{s}_1 & \bar{s}_1 & -\bar{s}_2 & \bar{s}_2 \\ -\bar{s}_3 & -\bar{s}_3 & -\bar{s}_4^* & -\bar{s}_4^* & -\bar{s}_1^* & \bar{s}_1^* & \bar{s}_2^* & \bar{s}_2^* \\ \bar{s}_4^* & -\bar{s}_4^* & -\bar{s}_3 & \bar{s}_3 & \bar{s}_2 & -\bar{s}_2 & \bar{s}_1 & \bar{s}_1 \\ -\bar{s}_4 & -\bar{s}_4 & \bar{s}_3^* & \bar{s}_3^* & -\bar{s}_2^* & -\bar{s}_2^* & -\bar{s}_1^* & \bar{s}_1^* \end{bmatrix} \quad (39)$$

Detailed decoding metrics for these codes can be found in the following sections.

A. MISO system

First, we consider a MISO system using the Alamouti code with PSK or QAM modulation schemes, and with only one Rx antenna. For simplicity, we denote the channel coefficient vectors between the Tx antennas and the Rx antenna to be \bar{h}_m , for $m = 1, 2$. The decoding metrics for the MB-OFDM symbols are presented in Table II.

Clearly, from Table II, the data at each sub-carrier can be decoded separately, rather than jointly. Therefore, the decoding metrics for data at the k -th sub-carrier, for $k = 1, \dots, N_D$, in the MB-OFDM symbols \bar{s}_1 and \bar{s}_2 are

$$\begin{aligned} s_{1,k} &= \arg \min_{s \in \mathcal{C}} [|(\bar{h}_{1,k}^* \mathbf{r}_{1,k} + \bar{h}_{2,k} \mathbf{r}_{2,k}^*) - s|^2 + \\ &\quad (-1 + \sum_{m=1}^2 |\bar{h}_{m,k}|^2) |s|^2] \quad (40) \\ s_{2,k} &= \arg \min_{s \in \mathcal{C}} [|(\bar{h}_{2,k}^* \mathbf{r}_{1,k} - \bar{h}_{1,k} \mathbf{r}_{2,k}^*) - s|^2 + \\ &\quad (-1 + \sum_{m=1}^2 |\bar{h}_{m,k}|^2) |s|^2]. \end{aligned}$$

For the DCM scheme, the decoding process is slightly more complicated, compared to PSK or QAM modulation schemes. A pair of data points $s_{m,k}$ and $s_{m,k+50}$, where $s_{m,k}$ and $s_{m,k+50}$ are the data points within the MB-OFDM symbol

TABLE IV
SIMULATION PARAMETERS.

Parameter	Value
FFT and IFFT size	$N_{fft} = 128$
Data rate	320 Mbps
Convolutional encoder's rate	1/2
Convolutional encoder's constraint length	$K = 7$
Convolutional decoder	Viterbi
Decoding mode	Hard
Number of transmitted MB-OFDM symbols	1200
Modulation	QPSK & DCM
IEEE Channel model	CM1, 2, 3 & 4
Number of data subcarriers	$N_D = 100$
Number of pilot subcarriers	$N_P = 12$
Number of guard subcarriers	$N_G = 10$
Total number of subcarriers used	$N_T = 122$
Number of samples in ZPS	$N_{ZPS} = 37$
Total number of samples/symbol	$N_{SYM} = 165$
Number of channel realizations	100

\bar{s}_m and are separated from each other by 50 tones, must be simultaneously decoded. For instance, decoding metrics for $s_{1,k}$ and $s_{1,k+50}$, for $k = 1, \dots, N_D/2$, are as follows

$$\begin{aligned} [s_{1,k}, s_{1,k+50}] &= \arg \min_{s \in \mathcal{C}_{DCM}, s_{50} \in \mathcal{C}_{DCM,50}} \\ & [|(\bar{h}_{1,k}^* \mathbf{r}_{1,k} + \bar{h}_{2,k} \mathbf{r}_{2,k}^*) - s|^2 + \\ & |(\bar{h}_{1,k+50}^* \mathbf{r}_{1,k+50} + \bar{h}_{2,k+50} \mathbf{r}_{2,k+50}^*) - s_{50}|^2 \\ & + (-1 + \sum_{m=1}^2 |\bar{h}_{m,k}|^2) |s|^2 + (-1 + \sum_{m=1}^2 |\bar{h}_{m,k+50}|^2) |s_{50}|^2] \quad (41) \end{aligned}$$

where the complex space \mathcal{C}_{DCM} denotes all potential possibilities that the symbol s can take, while the complex space $\mathcal{C}_{DCM,50}$ denotes all potential possibilities that the symbol s_{50} can take. The exact values of \mathcal{C}_{DCM} and $\mathcal{C}_{DCM,50}$ can be found in [19].

Similarly, for the code \mathbf{S}_8 , we can easily derive the decoding metrics of the MB-OFDM symbols \bar{s}_1 , \bar{s}_2 , \bar{s}_3 , and \bar{s}_4 by slight modification from the detailed decoding metrics mentioned in [18] for this CO STBC in conventional STC MIMO systems, and arrive at the decoding metrics in Table III. Hence, the data point $s_{m,k}$ at the k -th tone, for $k = 1, \dots, N_D$, can be decoded separately. For instance, the decoding metric for the data $s_{1,k}$ is

$$\begin{aligned} s_{1,k} &= \arg \min_{s \in \mathcal{C}} [|(\bar{h}_{8,k}^* \mathbf{r}_{7,k} + \bar{h}_{6,k}^* \mathbf{r}_{5,k} + \bar{h}_{7,k}^* \mathbf{r}_{7,k} + \\ & \bar{h}_{3,k}^* \mathbf{r}_{3,k} + \bar{h}_{1,k}^* \mathbf{r}_{1,k} + \bar{h}_{6,k} \mathbf{r}_{6,k}^* + \bar{h}_{2,k}^* \mathbf{r}_{1,k} - \\ & \bar{h}_{5,k} \mathbf{r}_{6,k}^* + \bar{h}_{2,k} 2\mathbf{r}_{2,k}^* - \bar{h}_{1,k} \mathbf{r}_{2,k} + \bar{h}_{5,k}^* \mathbf{r}_{5,k} + \\ & \bar{h}_{4,k}^* \mathbf{r}_{3,k} - \bar{h}_{3,k} \mathbf{r}_{4,k} + \bar{h}_{4,k} \mathbf{r}_{4,k} - \bar{h}_{7,k} \mathbf{r}_{8,k} + \\ & \bar{h}_{8,k} \mathbf{r}_{8,k}^*) - s|^2 + (-1 + 2 \sum_{m=1}^8 |\bar{h}_{m,k}|^2) |s|^2] \quad (42) \end{aligned}$$

A deduction similar to (42) is applied for the data $s_{2,k}$, $s_{3,k}$, and $s_{4,k}$ in PSK or QAM schemes. Accordingly, a deduction as in (42) can be applied for \mathbf{S}_8 with the DCM scheme.

B. MIMO system

Next, we consider the MIMO system with N Rx antennas. Linear combinations of the received signals from N Rx antennas are used to decode the transmitted symbols. Therefore,

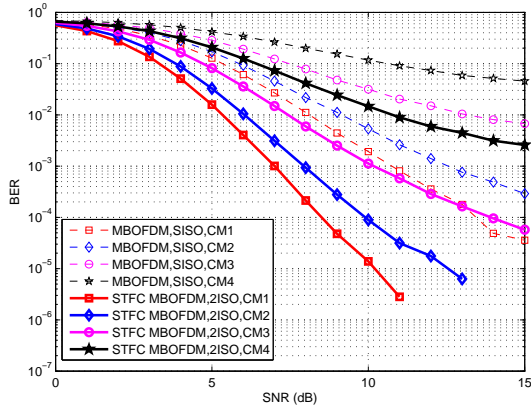


Fig. 5. Alamouti STFC MB-OFDM UWB performance with QPSK modulation/demodulation, and with 1 Rx antenna.

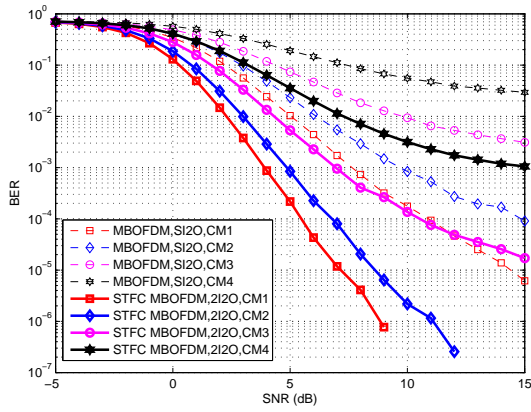


Fig. 6. Alamouti STFC MB-OFDM UWB performance with QPSK modulation/demodulation, and with 2 Rx antennas.

the decoding metrics for the transmitted symbol vectors \bar{s}_1 , \bar{s}_2 , \bar{s}_3 , and \bar{s}_4 can be deduced simply by replacing \bar{h}_m , for $m = 1, \dots, M$, in Tables II and III by the term $\bar{h}_{m,n}$, while replacing $\|\cdot\|_F^2$ with $\sum_{n=1}^N \|\cdot\|_F^2$. Similar to MISO systems, each data point can be separately decoded.

VII. SIMULATION RESULTS

To examine the performance of the proposed STFC MB-OFDM UWB systems, we used the codes S_2 in (38) and S_8 in (39), and ran several Monte-Carlo simulations, each with 1200 MB-OFDM symbols. As suggested in [15], 100 channel realizations of each IEEE 802.15.3a channel models (CM 1, 2, 3 and 4) were considered for the transmission of each MB-OFDM symbol. In simulations, SNR is defined to be the signal-to-noise ratio (dB) per sample in a MB-OFDM symbol (consisting of 165 samples), at each Rx antenna. It means that, at a certain Rx antenna, SNR is the subtraction between the total power (dB) of the received signal corresponding to the sample of interest and the power of noise (dB) at that Rx antenna. To fairly compare the error performance of MB-OFDM systems with and without STFCs, the average power of the signal constellation points in the STFC MB-OFDM

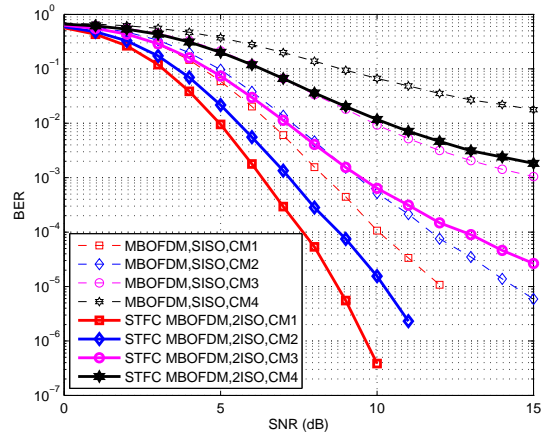


Fig. 7. Alamouti STFC MB-OFDM UWB performance with DCM modulation/demodulation, and with 1 Rx antenna.

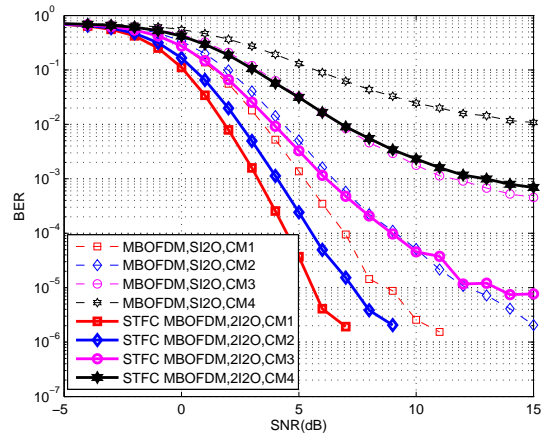


Fig. 8. Alamouti STFC MB-OFDM UWB performance with DCM modulation/demodulation, and with 2 Rx antennas.

system is scaled down by a factor of $1/M$, which is $1/2$ for the Alamouti code and $1/8$ for our order-8 code. Thereby, the average transmitting power from all M Tx antennas at a certain time is kept the same for both MB-OFDM systems with and without STFCs. Both modulation schemes QPSK and DCM are simulated. The simulation parameters are listed in Table IV.

The simulation results show that a significant improvement in bit error ratios (BER) can be achieved with the proposed STFC MB-OFDM system, compared to the conventional MB-OFDM system. Fig. 5 shows that an improvement of at least 5 dB at $BER = 10^{-4}$ can be achieved in the Alamouti STFC MB-OFDM 2ISO system (2 Tx, 1 Rx antennas), compared to the conventional MB-OFDM SISO system (1 Tx, 1 Rx antennas) with a QPSK scheme. Fig. 6 shows that a similar improvement as above can also be achieved in the Alamouti STFC MB-OFDM 2I2O system compared to the conventional MB-OFDM SI2O system. By comparing Figs. 5 and 6, the use of two Rx antennas advances the error performance of MB-OFDM systems (with or without STFCs) by approximately 3 dB at $BER = 10^{-4}$, compared to that of a MB-OFDM

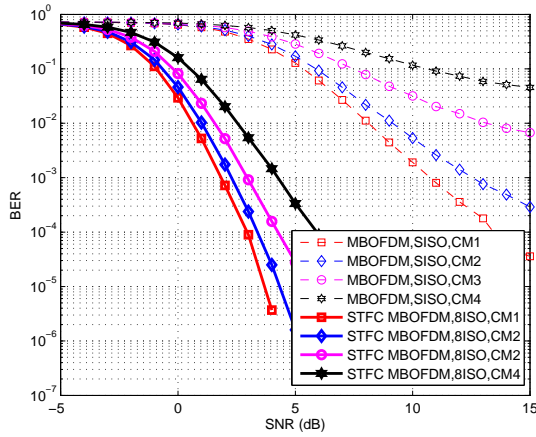


Fig. 9. Order-8 STFC MB-OFDM UWB performance with QPSK modulation/demodulation, and with 1 Rx antenna.

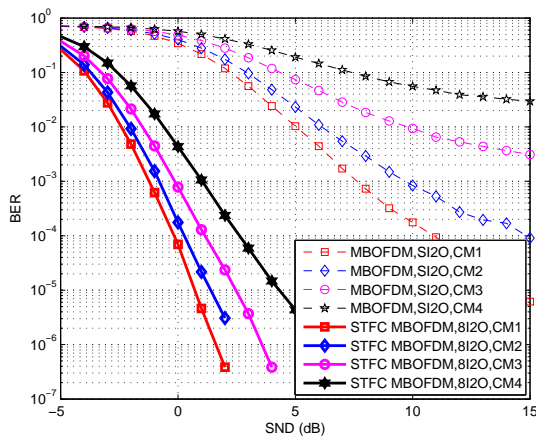


Fig. 10. Order-8 STFC MB-OFDM UWB performance with QPSK modulation/demodulation, and with 2 Rx antennas.

system (with or without STFCs, respectively) with only 1 Rx antenna.

Further, by comparing Fig. 7 with Fig. 5 (and Fig. 8 with Fig. 6), we can realize that the STFC MB-OFDM system associated with a DCM scheme provides a better performance of at least 1 dB at $BER = 10^{-4}$, compared to that associated with a QPSK scheme, due to the fact that DCM provides more time and frequency diversity than QPSK. A much bigger improvement can be observed in conventional MB-OFDM systems, in both cases of one and two Rx antennas.

Similarly, for the code S_8 , Fig. 9 shows that an improvement of at least 11 dB at $BER = 10^{-4}$ can be gained in the order-8 STFC MB-OFDM 8ISO system, compared to the conventional MB-OFDM SISO system with a QPSK scheme. In Fig. 10, the similar advance as above can be achieved in the order-8 STFC MB-OFDM 8I2O system, compared to the conventional MB-OFDM Si2O system. By comparing these two figures, it is clear that the error performance of an MB-OFDM system (either with or without STFCs) can be advanced by approximately 3 dB at $BER = 10^{-4}$ when the number of Rx antennas is doubled.

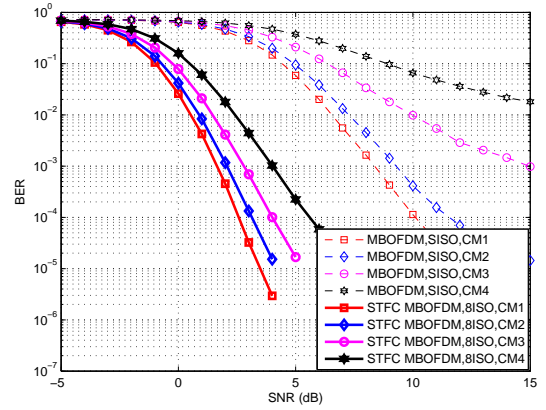


Fig. 11. Order-8 STFC MB-OFDM UWB performance with DCM modulation/demodulation, and with 1 Rx antenna.

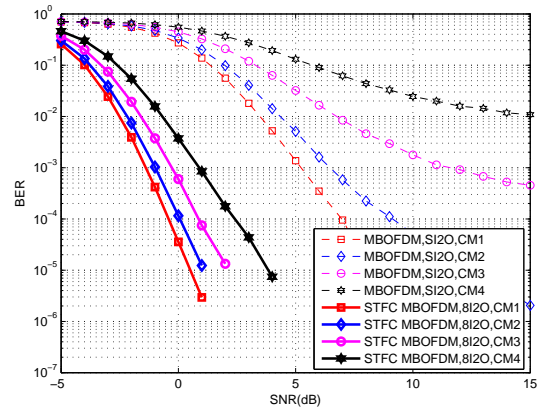


Fig. 12. Order-8 STFC MB-OFDM UWB performance with DCM modulation/demodulation, and with 2 Rx antennas.

Finally, by comparing Fig. 11 with Fig. 9 (and Fig. 12 with Fig. 10), the use of a DCM scheme provides slightly better error performance to STFC MB-OFDM systems. However, a great improvement of at least 3.5 dB can be achieved at $BER = 10^{-4}$ in conventional MB-OFDM systems, and in both cases of one and two Rx antennas.

VIII. CONCLUSIONS

The paper proposes a general STFC MB-OFDM UWB model. A great similarity between the STFC MB-OFDM UWB systems and conventional wireless STBC MIMO systems is discovered. This similarity allows the authors to derive a) the PEP, b) the diversity gain and coding gain, c) the design criteria for STFCs, and d) the general decoding method for STFCs implemented in MB-OFDM UWB systems. The analysis is carried out directly for the log-normal distribution of UWB multipath amplitudes in a general scenario, without any restriction on the time delay and average power of transmit-receive links as in [12].

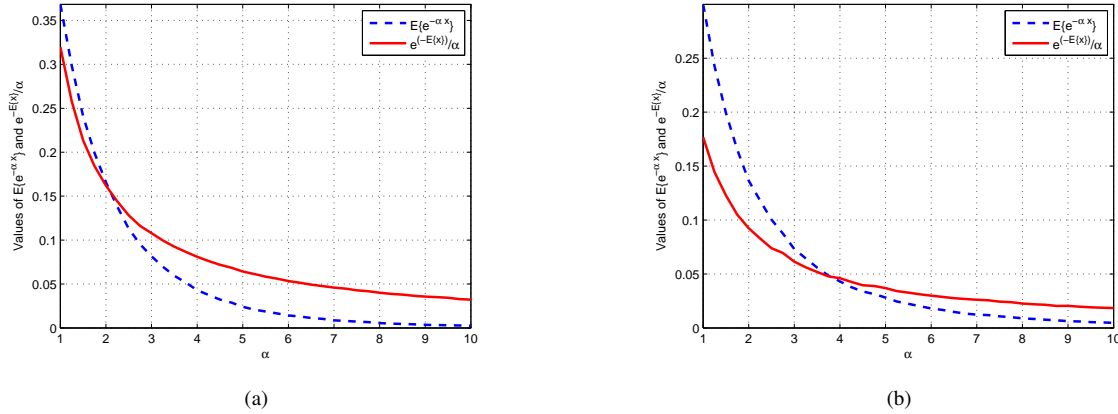


Fig. 13. $E\{e^{-\alpha x}\}$ and $\frac{1}{\alpha}e^{-E\{x\}}$ as functions of α . (a) $\mu = 0$, $\sigma = 0.5$. (b) $\mu = 0.25$, $\sigma = 0.75$.

APPENDIX I PROOF OF INEQUALITY

In this appendix, we consider the term $E\{e^{-\alpha x}\}$, where α is a positive coefficient and x is a log-normally distributed RV $x \sim \text{Log} - N(\mu, \sigma^2)$. We will prove that

$$E\{e^{-\alpha x}\} \leq \frac{1}{\alpha}e^{-E\{x\}}, \quad (43)$$

when α is large enough.

By definition, $E\{e^{-\alpha x}\}$ can be quantified as

$$E\{e^{-\alpha x}\} = \int_0^{\infty} e^{-\alpha x} p(x) dx, \quad (44)$$

where $p(x)$ is the pdf of the log-normally distributed RV x . Therefore, (43) becomes

$$\int_0^{\infty} \alpha e^{-\alpha x} p(x) dx \leq e^{-E\{x\}}. \quad (45)$$

Using the property [25]

$$\lim_{\alpha \rightarrow \infty} \alpha e^{-\alpha x} \rightarrow \delta(x),$$

where $\delta(x)$ is the Dirac delta distribution, we have

$$\begin{aligned} \lim_{\alpha \rightarrow \infty} \int_0^{\infty} \alpha e^{-\alpha x} p(x) dx &= \int_0^{\infty} \delta(x) p(x) dx \\ &= p(0). \end{aligned} \quad (46)$$

By definition of the log-normal distribution [17], we have $p(0) = 0$. Clearly, the left-hand side of (45) approaches zero when α goes to infinity, while the right-hand side is a positive constant. Therefore, the inequality (45) (and thus (43)) holds when α is large enough, i.e. $\alpha \geq \alpha_0$, where α_0 is a function of μ and σ^2 . The inequality (43) has been proved. ■

Example 1: For illustration, the simulation 13(a) shows the values of $E\{e^{-\alpha x}\}$ and $\frac{1}{\alpha}e^{-E\{x\}}$ as functions of α for the case $\mu = 0$, $\sigma = 0.5$. We realize that $E\{e^{-\alpha x}\} \leq \frac{1}{\alpha}e^{-E\{x\}}$ when $\alpha \geq 2.1$.

Example 2: We present another example for $\mu = 0.25$, $\sigma = 0.75$. Fig. 13(b) shows that $E\{e^{-\alpha x}\} \leq \frac{1}{\alpha}e^{-E\{x\}}$ when $\alpha \geq 3.8$.

ACKNOWLEDGMENT

The authors are grateful to Prof. Vahid Tarokh, Harvard University, U.S.A for helpful advices about distribution and PEP; Assoc. Prof. Xiaojing Huang and Assoc. Prof. Tadeusz A. Wysocki, University of Wollongong, Australia for the helpful comments about the OAAO and the appendix; Prof. Lutz Mattner, University of Luebeck, Germany, for his help with the proof of the inequality (43); Assoc. Prof. Tan-Hsu Tan and Mr. Kuan-Chih Lin for helping us to have deep understanding of their work [11]; and anonymous reviewers for insightful comments.

REFERENCES

- [1] A. Batra et al., "Multiband OFDM physical layer specification," *WiMedia Alliance*, Release 1.1, July 2005.
- [2] I. E. Telatar, "Capacity of multi-antenna Gaussian channels," *European Trans. Telecom.*, vol. 10, no. 6, pp. 585–595, 1999.
- [3] G. J. Foschini, "Layered space-time architecture for wireless communication in a fading environment when using multi-element antennas," *Bell Labs Technical Journal*, vol. 1, no. 2, pp. 41–59, Autumn 1996.
- [4] G. J. Foschini and M. J. Gans, *On limits of wireless communications in a fading environment when using multiple antennas*, vol. 6 of 3, Wireless Communications, Printed in the Netherlands, Mar. 1998.
- [5] V. Tarokh, N. Seshadri, and A. R. Calderbank, "Space-time codes for high data wireless communications: performance criterion and code construction," *IEEE Trans. Inform. Theory*, vol. 44, no. 2, pp. 744 – 765, Mar. 1998.
- [6] Y. Gong and K. B. Letaief, "Space-time-frequency coded OFDM for broadband wireless communications," *Proc. IEEE Global Telecommunications Conference GLOBECOM '01*, vol. 1, pp. 519–523, Nov. 2001.
- [7] A. F. Molisch, M. Z. Win, and J. H. Winters, "Space-time-frequency (STF) coding for MIMO-OFDM systems," *IEEE Commun. Lett.*, vol. 6, no. 9, pp. 370–372, Sept. 2002.
- [8] Z. Liu, Y. Xin, and G. B. Giannakis, "Space-time-frequency coded OFDM over frequency-selective fading channels," *IEEE Trans. Sign. Process.*, vol. 50, no. 10, pp. 2465–2476, Oct. 2002.
- [9] M. Fozunbal, S. W. McLaughlin, and R. W. Schafner, "On space-time-frequency coding over MIMO-OFDM systems," *IEEE Trans. Wireless Commun.*, vol. 4, no. 1, pp. 320–331, Jan. 2005.
- [10] W. Su, Z. Safar, and K. J. R. Liu, "Towards maximum achievable diversity in sapce, time, and frequency: performance analysis and code design," *IEEE Trans. Wireless Commun.*, vol. 4, no. 4, pp. 1847–1857, July 2005.
- [11] T.-H. Tan and K.-C. Lin, "Performance of space-time block coded MB-OFDM UWB systems," *Proc. 4th Annual Communication Networks and Services Research Conference (CNSR'06)*, pp. 323 – 327, May 2006.
- [12] W.P. Siringopairat, W. Su, M. Olfat, and K.J.R. Liu, "Multiband-OFDM MIMO coding framework for UWB communication systems," *IEEE Trans. Sign. Process.*, vol. 54, no. 1, pp. 214 – 224, Jan. 2006.

- [13] J. Hou and M. H. Lee, "High rate ultra wideband space time coded OFDM," *Proc. 58th IEEE Veh. Technol. Conf. VTC 2003 - Fall*, vol. 4, pp. 2449–2451, Oct. 2003.
- [14] J. Wang, G. Zhu, and J. Jin, "Optimal power allocation for space-time coded OFDM UWB systems," *Proc. IEEE Int. Conf. Wireless Communications, Networking and Mobile Computing WCNM.2005*, vol. 1, pp. 189–192, Sept. 2005.
- [15] J. Foerster et. al., "Channel modelling sub-committee report final," *IEEE P802.15 Working Group for Wireless Personal Area Networks (WPANs), IEEE P802.15-02/490r1-SG3a*, Oct. 2005.
- [16] S. M. Alamouti, "A simple transmit diversity technique for wireless communications," *IEEE J. Select. Areas Commun.*, vol. 16, no. 8, pp. 1451–1458, Oct. 1998.
- [17] E. L. Crow and K. Shimizu (Ed.), *Lognormal distributions*, vol. 88, Marcel Dekker, Inc, New York, 1988.
- [18] L. C. Tran, T. A. Wysocki, A. Mertins, and J. Seberry, *Complex Orthogonal Space-Time Processing in Wireless Communications*, Springer, New York, USA, 2006.
- [19] A. Batra et al., "Multi-band OFDM physical layer proposal for IEEE 802.15 task group 3a," *IEEE P802.15-04/0493r1*, Sept. 2004.
- [20] A. Batra, J. Balakrishnan, G. R. Aiello, J. R. Foerster, and A. Dabak, "Design of a multiband OFDM system for realistic UWB channel environments," *IEEE Trans. on Microwave Theory and Techniques*, vol. 52, no. 9, pp. 2123–2138, Sept. 2004.
- [21] V. Tarokh, H. Jafarkhani, and A. R. Calderbank, "Space-time blocks codes from orthogonal designs," *IEEE Trans. Inform. Theory*, vol. 45, no. 5, pp. 1456–1467, July 1999.
- [22] V. Tarokh, H. Jafarkhani, and A. R. Calderbank, "Space-time block coding for wireless communications: performance results," *IEEE J. Select. Areas Commun.*, vol. 17, no. 3, pp. 451–460, Mar. 1999.
- [23] L. F. Fenton, "The sum of log-normal probability distributions in scatter transmission systems," *IRE Trans. Commun. Syst.*, vol. CS-8, pp. 57–67, 1960.
- [24] X.-B. Liang, "Orthogonal designs with maximal rates," *IEEE Trans. Inform. Theory*, vol. 49, no. 10, pp. 2468–2503, Oct. 2003.
- [25] L. W. Couch, *II: Digital and analog communication systems*, vol. 6, Prentice Hall, Upper Saddle River, 2001.